Thermodiffusion in a multicomponent lyotropic mixture in the vicinity of the critical micellar concentration by using the *Z*-scan technique

M. P. Santos
Instituto de Física, Universidade de São Paulo, caixa postal 66318, 05315-970, São Paulo, São Paulo, Brazil

S. L. Gómez*
Instituto de Física, Universidade de São Paulo, caixa postal 66318, 05315-970, São Paulo, São Paulo, Brazil

E. Bringuier
Matériaux et Phénomènes Quantiques (Unité mixte 7162 du CNRS), Université Denis Diderot (Paris 7), 10 rue Alice Domont et Léonie Duquet, 75205 Paris Cedex 13, France

A. M. Figueiredo Neto
Instituto de Física, Universidade de São Paulo, caixa postal 66318, 05315-970, São Paulo, São Paulo, Brazil
(Received 5 March 2007; revised manuscript received 20 September 2007; published 23 January 2008)

Thermodiffusion in a lyotropic mixture of water and potassium laurate is investigated by means of an optical technique (*Z* scan) distinguishing the index variations due to the temperature gradient and the mass gradients. A phenomenological framework allowing for coupled diffusion is developed in order to analyze thermodiffusion in multicomponent systems. An observable parameter relating to the mass gradients is found to exhibit a sharp change around the critical micellar concentration, and thus may be used to detect it. The change in the slope is due to the markedly different values of the Soret coefficients of the surfactant and the micelles. The difference in the Soret coefficients is due to the fact that the micellization process reduces the energy of interaction of the ball of amphiphilic molecules with the solvent.

DOI: 10.1103/PhysRevE.77.011403 PACS number(s): 82.70.−y, 66.90.+r, 78.20.Nv, 47.57.−s

I. INTRODUCTION

In the physical chemistry of self-assembled amphiphile-solvent systems, the concept of the *critical micellar concentration* (CMC) [1] is one of the most interesting from both the fundamental and technological points of view. Let us consider, for example, a lyotropic-type mixture [2] of a surfactant and water. The CMC is defined as the molar concentration of amphiphilic molecules (c) above which they self-assemble into micelles. When c is greater than the CMC, the concentration of micelles increases and that of isolated amphiphilic molecules remains almost constant.

Different theoretical approaches have been used for the understanding of the micellization process [1,3–6]. From the experimental point of view, some properties of amphiphile solutions, such as detergency, equivalent electrical conductivity, high-frequency conductivity, surface tension, osmotic pressure, and interfacial tension, exhibit a remarkable behavior as the amphiphile concentration approaches the CMC [7]. In actual mixtures, there is no uniquely defined concentration of amphiphiles at which all these properties present a drastic modification in their behavior.

More recently, nonlinear optical properties of amphiphilic solutions were investigated at amphiphile concentrations around the CMC. Using a mixture of potassium laurate [$COOK(CH_2)_{10}CH_3$] (KL) and water, it has been shown [8] that the presence of micelles in the solution changes the behaviors of the thermo-optic coefficient and of the nonlinear index of refraction with respect to those of the system when c is below the CMC.

The Soret or Ludwig-Soret effect [9,10], also called thermodiffusion or thermal diffusion, designates a flow of matter driven by a temperature gradient. In a binary fluid mixture, characterized by a mass fraction φ of one of its components, subjected to a temperature gradient, a flow of matter is observed for this component in the fluid, parallel to the temperature gradient. The Ludwig-Soret effect couples the flow of matter to the temperature gradient in the system. Besides its fundamental interest in physical chemistry, this phenomenon also has technological applications [11,12].

The Soret effect for colloidal dispersions, measured by the Soret coefficient S_T, is 10^2-10^3 times stronger than that observed in molecular systems such as mixtures of gases and liquids [13]. Depending on the system, the Soret effect may be thermophobic (when colloidal particles tend to gather in the colder part of the sample) or thermophilic. Different experimental techniques can be used to measure S_T, e.g., the thermogravitational column [14], forced Rayleigh scattering [15,16], and more recently single-beam *Z* scan (ZS) [17,18], thermal lensing [19], and thermal pumping and fluorescence [20].

Although some efforts have been made to investigate the Soret effect in micellar systems [21–24], to the best of our knowledge, there is not in the literature a systematic study of the thermodiffusion phenomenon around the CMC in a lyotropic mixture. In other words, what are the behaviors of the concentration gradients of free amphiphilic molecules and

*Present address: Universidade Estadual de Ponta Grossa, Campus Uvaranas, Avenida Carlos Cavalcanti, 4748, 4030-900, Ponta Grossa, Paraná, Brazil.

micelles due to the temperature gradient, as the CMC is crossed? If the thermodiffusion phenomenon is sensitive to the transformation from free molecules to micelles, it could be used to determine the CMC.

A complication exists in the study of thermodiffusion in micellar systems: the system is at least ternary, with the solvent, the free amphiphilic molecules, and the micelles. In such a system, the usual phenomenological framework in which the Soret coefficient is defined cannot be straightforwardly applied. That complication is present in all complex fluids; hence the need to implement a more general framework in order to deal with thermodiffusion in complex fluids.

The present paper thus serves two purposes. The first one is to extend an experimental technique originally devised for binary mixtures, and the second one is to evidence micellization using a physical property not investigated heretofore. Discussing specific quantitative theories of thermodiffusion or of the micellization process is outside the scope of this paper. Specifically, we shall use the ZS technique to investigate thermodiffusion in a mixture of amphiphilic molecules and a solvent, as a function of the amphiphile concentration. The paper is organized as follows. Section II outlines the phenomenological framework for handling thermodiffusion in a multicomponent fluid. That framework is used to extend the ZS technique to a multicomponent fluid. (Details about our phenomenological equations of thermodiffusion are provided in the Appendixes.) Then, Sec. III describes the technical aspects of the experiments and the samples studied. The results are presented in Sec. IV, which shows how transport coefficients can be extracted from the optical signal. The interpretation of the Soret response shows that it is consistent with the present knowledge of the micellar system and of the thermodiffusion phenomenon. Conclusions are drawn in Sec. V.

II. PHENOMENOLOGICAL FRAMEWORK

In a binary mixture, the Soret coefficient S_T is defined as the relative slope of the steady-state profile of the denser component due to the temperature gradient as $S_T=-\nabla\varphi/(\varphi\nabla T)$, where T is the absolute temperature and φ is the mass fraction. As the current density J of the denser component is a linear combination of $\nabla\varphi$ and $\varphi\nabla T$, namely, $J=-D\nabla\varphi-D_T\varphi\nabla T$ [9,10],

$$S_T = D_T/D, \tag{1}$$

where D_T and D are the thermodiffusion coefficient (in $m^2\ s^{-1}\ K^{-1}$) and the ordinary diffusion coefficient (in $m^2\ s^{-1}$), respectively [25]. That current equation is expected to hold in the dilute limit $\varphi \ll 1$, with constant (i.e., φ-independent) diffusion and thermodiffusion coefficients.

Let us define the Soret function of the solute as $F_S(\varphi)=-\nabla\varphi/\nabla T$ (in a previous work [26], we named this function the *concentration-dependent Soret coefficient*). It is a function of φ at fixed T. By measuring $F_S(\varphi)$, one can verify that it is proportional to φ.

In the case of a multicomponent mixture (of more than two components), the phenomenological formulation of the problem becomes more complex [27,28]. Leahy-Dios and co-workers [29] recently measured the ordinary diffusion and thermodiffusion coefficients of ternary mixtures using the thermogravitational-column technique. In a ternary or more complex mixture, we shall retain the operational definition of the Soret function of the solute i as

$$F_{S,i} = -\nabla\varphi_i/\nabla T \tag{2}$$

in the steady state. That function now depends not only on φ_i but also on the φ_j of the other solutes $j\neq i$. This comes about because the ordinary diffusions of the solutes are coupled by nondiagonal diffusion coefficients D_{ij}. Based on the phenomenological laws of multicomponent diffusion and thermodiffusion, Appendix A expresses the expected dependence of $F_{S,i}$ on the φ_j's.

In a ZS experiment, the sample is illuminated by a Gaussian laser beam, giving rise to a change in the index of refraction $\delta n(r,t)$ where r and t are the radial distance to the beam axis and the time. The change δn is due to the dependence of n on the incident intensity I (nonlinear optical effect), on the temperature T, and on the local solute mass fractions $\varphi_1(r,t)$, $\varphi_2(r,t)$, and so on. If δn is small, it can be written as a linear expansion:

$$\delta n(r,t) = \left(\frac{\partial n}{\partial I}\right) I(r,t) + \left(\frac{\partial n}{\partial T}\right)\delta T(r,t) + \left(\frac{\partial n}{\partial \varphi_1}\right)\delta\varphi_1(r,t) + \left(\frac{\partial n}{\partial \varphi_2}\right)\delta\varphi_2(r,t) + \cdots. \tag{3}$$

That expansion is the generalization of the one used in previous work [18,30], where only one solute was present. Here, the mass-fraction changes $\delta\varphi_i$ are caused by the Soret effect, according to $\delta\varphi_i=(\nabla\varphi_i/\nabla T)\delta T$. In the steady state or, more generally, in the quasisteady state used in the two-time-scale analysis [16], we have $\delta\varphi_i=-F_{S,i}\delta T$, where $F_{S,i}$ is the Soret function of solute i. As the lensing effect is due to

$$\delta n(r,t) = \left(\frac{\partial n}{\partial I}\right) I(r,t) + \left[\left(\frac{\partial n}{\partial T}\right) - \left(\frac{\partial n}{\partial \varphi_1}\right)F_{S,1} - \left(\frac{\partial n}{\partial \varphi_2}\right)F_{S,2} + \cdots\right]\delta T(r,t), \tag{4}$$

the ZS optical signal involves the Soret functions $F_{S,i}$ of the N solutes through the following linear combination:

$$\Xi = \sum_{i=1}^{N} F_{S,i}\left(\frac{\partial n}{\partial \varphi_i}\right). \tag{5}$$

As we shall see shortly, the ZS method is able to distinguish the temperature-lens contribution to δn and the matter-lens contribution, proportional to Ξ. The experiment does not discriminate the contributions in Ξ. In Sec. IV, the measured $\Xi(\varphi_1,\varphi_2,\ldots)$ is equated to a phenomenological expression involving the transport parameters of the mobile species, and those parameters are inferred from $\Xi(\varphi_1,\varphi_2,\ldots)$.

During the ZS experiment, the sample is illuminated by a laser beam during a time period Δt. The time constants associated with the thermal lens (t_c) and the thermal diffusion phenomena (t_{so}) for dye-doped lyotropics (we will come

back to this point later on) are of the order of 5 ms and 5 s, respectively. So, for laser pulse widths (exposition) $t_c < \Delta t < t_{so}$ (in our case, $\Delta t \sim 40$ ms), φ in the illuminated sample volume is expected to be approximately constant along the z direction (sample thickness much smaller than the Rayleigh length of the laser Gaussian beam).

For $t_c < \Delta t < t_{so}$, the optical transmitted intensity $\Gamma(z,t)$ in the far field in a ZS experiment is written as [18]

$$\Gamma(z,t) = \frac{\Gamma'}{1 - 2\gamma\left(\frac{C_N}{(1+\gamma^2)^2} + \frac{C_T}{1+\gamma^2}\frac{t}{t+2t_c}\right) + (1+\gamma^2)\left(\frac{C_N}{(1+\gamma^2)} + \frac{C_T}{1+\gamma^2}\frac{t}{t+2t_c}\right)^2}, \tag{6}$$

where Γ' is the sample transmitted intensity when the sample is at $|z| \gg z_0$, at any time $t \leq \Delta t$, $\gamma = z/z_0$, C_N, and C_T are dimensionless parameters defined as

$$C_N = \frac{8bz_0P}{\pi\omega_0^4}\frac{\partial n}{\partial I}, \tag{7}$$

$$C_T = \frac{bz_0\alpha P}{\pi\omega_0^2\kappa}\frac{\partial n}{\partial T}, \tag{8}$$

where P, α, b, κ, and ω_0 are the incident power, the linear absorption coefficient, the sample thickness, the thermal conductivity, and the beam waist at the focus.

For $\Delta t > t_{so}$, the optical transmitted intensity $\Gamma(z)$ in the far field in a ZS experiment is written as [30]:

$$\Gamma(z) = \frac{\Gamma'}{1 - 2\gamma A + (1+\gamma^2)A^2}, \tag{9}$$

with

$$A = \frac{C_N}{(1+\gamma^2)^2} + \frac{C_T}{1+\gamma^2} + \frac{C_S\tau}{(1+\gamma^2)(\tau+2t_c)}, \tag{10}$$

where $\tau = 2\Delta t$ and the dimensionless parameter C_S is, for a binary mixture,

$$C_S = -\frac{bz_0\alpha P}{2\pi\kappa\omega_0^2}F_S(\varphi)\frac{\partial n}{\partial \varphi}. \tag{11}$$

At this point we will generalize Eq. (11) to account for multicomponent mixtures (i.e., a solvent and N solutes), on the basis of Eq. (4). Therefore C_S can be expressed as

$$C_S = -\frac{bz_0\alpha P}{2\pi\kappa\omega_0^2}\left(\sum_{i=1}^{N} F_{S,i}\frac{\partial n}{\partial \varphi_i}\right) = -\frac{bz_0\alpha P}{2\pi\kappa\omega_0^2}\Xi. \tag{12}$$

Note that, if c_i denotes the molar concentration of component i, $\varphi_i(\partial n/\partial\varphi_i) = c_i(\partial n/\partial c_i)$.

The normalized transmitted intensity is defined by

$$\Gamma_N(z,t_s) = \frac{\Gamma(z,t_s)}{\Gamma'}, \tag{13}$$

and $\Gamma_N(z,t_s)$ exhibits a typical peak-valley behavior versus z, with a peak-to-valley amplitude where t_s is the time for which the transmitted intensity reaches a saturation value ($t_c < t_s < \Delta t$).

In this framework, C_T is determined independently and two scans are needed to obtain C_S: the first one with $t_c < \Delta t < t_{so}$, determines C_N, and a second run, with $\Delta t \geqq t_{so}$, determines C_S. The contributions of the nonlinear, temperature, and matter lenses are additive in Eq. (10), but they are not in Eq. (9) since Γ is a nonlinear function of A. Section IV B will show on a specific example how $\Gamma_N(z,t_s)$ depends on C_N, C_T, and C_S.

III. EXPERIMENT

The sample investigated is a mixture of potassium laurate and distilled and deionized water. Potassium laurate was synthesized from lauric acid (Merck) and recrystallized three times in absolute ethanol (Merck). The KL concentration (c) was varied from 2.46×10^{-3} M to 3.2×10^{-1} M. For $c > c_c = 24\times10^{-3}$ M (where c_c is the CMC) [31], corresponding to $\varphi_c = 6\times10^{-3}$, KL molecules form spherical micelles. At the highest KL concentration, which is about $10c_c$, we expect the molar concentration of free KL molecules to be still much larger than that of micellar KL. The errors in weighting are smaller than 0.5%. Samples were used within 2 days after preparation. All the measurements were performed at 23 °C.

As the lyotropic light absorption, at the wavelength used in our experiment, is very low (typically $\alpha_{ly} = 10^{-3}$ cm^{-1} at $\lambda = 532$ nm), the Congo Red (CR) dye (Aldrich Co., purity >91%, molecular mass 696.665) was added to the mixture. The dye, used to increase the sample absorption coefficient, is added at the fixed concentration of 40 μM in all the samples. At this concentration we have about 1.4×10^6 water molecules per CR molecule in the sample. The typical mass fraction of the CR molecules is 2.8×10^{-5}. We have checked that, at this concentration, CR modifies only the optical absorption of the mixture but not the phase sequence of the mixture. The absorbance spectra of the CR were measured in pure water and in solutions of KL at concentrations smaller and larger than the CMC. Particularly in the visible region of the spectra ($450 \leqslant \lambda \leqslant 600$ nm), the CR absorbance did not exhibit a noticeable change, remaining the same within our experimental accuracy of about 0.4%. Concerning the phase diagram (temperature versus the KL concentration) of the lyotropic mixture with and without the CR, at least at the

concentration used in our experiments, the phase sequence boundaries did not change their loci, within our experimental accuracy. In this case, the accuracy in the temperature is about 0.2 °C and in the KL concentration is about 0.04 wt %.

The samples were prepared in a slab geometry, forming a 200-μm-thick film. Our experimental setup allows us to make automated measurements with temporal resolution. The laser beam (Millennia II, cw, $\lambda=532$ nm, from Spectra Physics) was modulated at millisecond (second) time scales by a mechanical chopper (shutter). The sample was scanned around the focal point by a translational unit. The chopper or shutter provides a square wave pulse, exhibiting a periodical succession of "on" and "off" states of equal Δt duration. The sample position z is fixed during a sequence of one on state and one off state. The experiment consists in measuring the sample transmitted intensity $\Gamma(z,t)$ as a function of time during the on period, at each (fixed) sample position z. A photodetector measured the transmitted intensity of the sample after a pinhole positioned on the beam propagation axis in the far-field condition. The signal acquisition was made by an oscilloscope and a GPIB board.

Our analysis depends on the characterization of the induced nonlinear, temperature, and matter lenses, which have different characteristic times. So it is necessary to make two Z-scan measurements on each sample. In the present case we choose the time intervals of $\Delta t=44$ ms and 4.4 s. Those values, which characterize the time constants of the different physical phenomena investigated, have to be experimentally obtained. In the case of ferrofluid samples [30] they are typically of the order of the millisecond and the second, respectively. In a typical ZS transmittance curve as a function of time (at fixed z) there is an initial increase (or decrease) of the transmittance, which tends to a constant limiting value. The time interval at each time scale is chosen as that when the limiting value of the transmittance is fully attained. The total time of a ZS experiment is about 10 and 40 min with the time intervals of 44 ms and 4.4 s, respectively.

In the planning of the experiment, an important point is the incident power of the laser beam on the sample. The incident power on the sample was set at $P=42$ mW. This value was chosen taking into account experimental conditions such as the absence of spherical aberration and of convection, and the condition that the transport coefficients measured should be independent of P. The other parameters used in the experiments are $b=200$ μm, $z_0=0.786\pm0.012$ cm, and $\omega_0=36.48\pm0.28$ μm.

The linear optical absorption (α) of the samples is measured with a uv-2800 single beam scanning uv-visible spectrophotometer (at $\lambda=532$ nm). The linear refractive index (n_0) and the thermo-optic coefficient ($\partial n/\partial T$) of the different samples (at $\lambda=589$ nm) are measured using an Abbe refractometer (Carl Zeiss) with a temperature-controlled device (thermal bath Brookfield TC 500−0.01 °C accuracy). The parameter $\partial n/\partial\varphi$ is also measured in the different samples investigated.

IV. RESULTS AND DISCUSSION

A. Aqueous solutions of CR

In this section, the Soret coefficient of the CR molecules in water is determined by using the ZS technique. This is a simpler case since only two types of molecule are present in the system. The ZS experiments, on both time intervals, gave the typical peak-valley curves. The measurements of $\Gamma_N(z,t=0^+)$, for $\Delta t=44$ ms, showed an almost constant value, in our experimental conditions, indicating that the fast absorption-relaxation phenomenon is very weak. From these results we evaluate $C_N<10^{-2}$. This value is, at least, two orders of magnitude smaller than those found in ferrofluids [26] and ferrolyotropic mixtures and, therefore, we may disregard the first term in the right-hand side of Eq. (10).

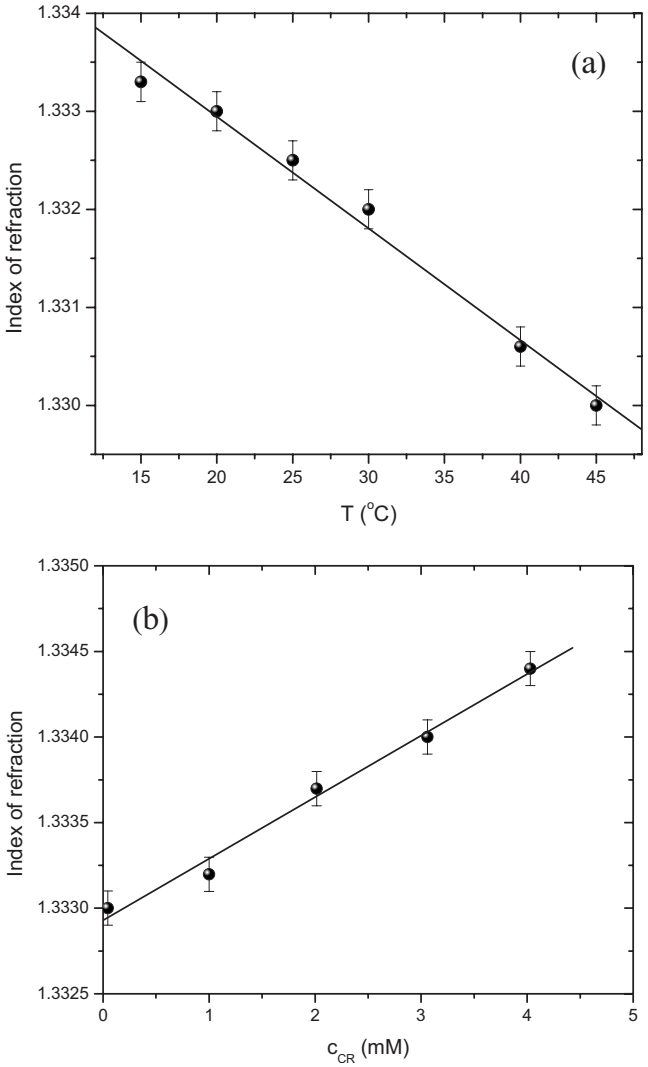

FIG. 1. Index of refraction of aqueous solutions of CR (a) as a function of the temperature at a fixed CR concentration, and (b) as a function of the CR concentration at a fixed temperature (23 °C).

Figure 1 shows the measured values of the refractive index of the aqueous solutions of CR as a function of the temperature [Fig. 1(a)] at a fixed CR concentration, and as a function of the CR concentration [Fig. 1(b)] at a fixed temperature (23 °C). The values of $\partial n/\partial T$ and $\partial n/\partial\varphi_{CR}$, where φ_{CR} is the mass fraction of the dye, are $-(1.07\pm0.07)\times10^{-4}$ K^{-1} and 0.511 ± 0.031, respectively, obtained from the best-fit procedure. The measured optical absorbance of an aqueous solution of CR at the fixed value $c_{CR}^{*}=40$ μM

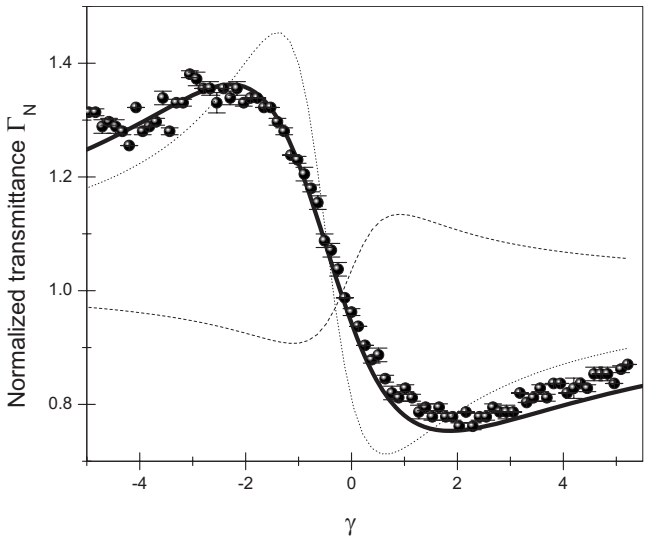

FIG. 2. Typical Z-scan experimental results of a lyotropic mixture of water, KL, and CR, with $\Delta t=4.4$ s and φ_{KL} (=1.127 $\times 10^{-3}$) below the CMC. γ is the position of the sample in units of z_0. The solid curve shows the prediction of Eq. (9) with $C_N=0$, $C_T=-0.359$, and $C_S=0.112$ as obtained from the scan. The dotted (dashed) curve shows the prediction of Eq. (9) with $C_N=0$, $C_T=-0.359$, and $C_S=0$ ($C_N=0$, $C_T=0$, and $C_S=0.112$).

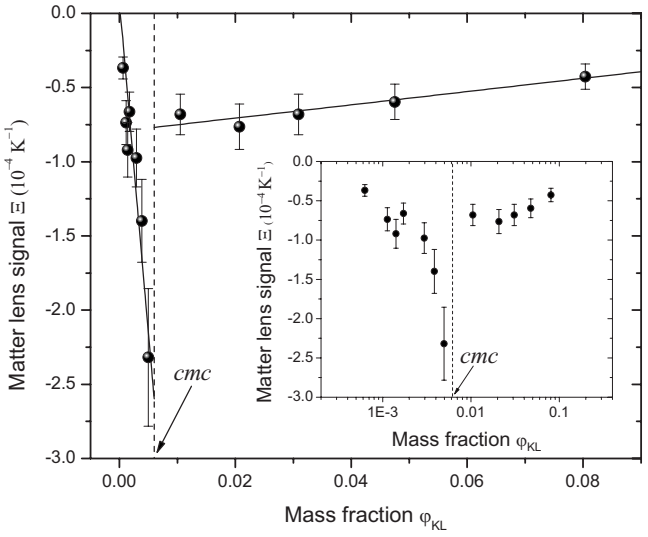

FIG. 3. Matter-lens signal Ξ as a function of the total KL mass fraction. The vertical dashed line represents the CMC. The solid lines represent linear fits to data. The inset shows the same data, with a semilogarithmic scale for the KL mass fraction.

(which corresponds to $\varphi_{CR}^*=2.8\times 10^{-5}$) is 1.18 ± 0.02 cm^{-1}, and we used $\kappa_w=0.6$ W m^{-1} K^{-1} of water. With these values we can calculate the nondimensional parameter C_T for the aqueous solution of the dye. To obtain C_S we followed the procedure described in Ref. [26]. As we are dealing here with a binary mixture, Eq. (11) is written

$$C_S = -\frac{bz_0\alpha P}{2\pi\kappa\omega_0^2} S_{T,CR}\varphi_{CR}^* \frac{\partial n}{\partial \varphi_{CR}}, \tag{14}$$

where $S_{T,CR}=D_{T,CR}/D_{CR}$ is the Soret coefficient of the dye. We found $S_{T,CR}=0.75\pm 0.12$ K^{-1}.

B. Aqueous solutions of KL and CR

Figure 2 shows a typical ZS experimental result $\Gamma_N(z,t_s)$ of a lyotropic mixture of water, KL, and CR, with φ_{KL} below the CMC, with $\Delta t=4.4$ s. Similar results are obtained for $\Delta t=44$ ms and above the CMC. In all of them, the peak-valley behavior is present. The solid line shows the prediction of Eq. (9) with C_N and C_S as obtained from two scans (the parameter C_T is obtained independently). We find that $C_N<10^{-2}$ and C_N is henceforth neglected in Eq. (10). The dotted and dashed lines in Fig. 2 show the prediction of Eq. (9) with other values of the parameters C_T and C_S. Thereby one can see how sensitive the normalized transmittance is to those parameters. Also here, the measurements of $\Gamma_N(z,t=0^+)$, for $\Delta t=44$ ms, showed an almost constant value, in our experimental conditions.

The ZS analysis of the thermal-lens signal allows us to isolate a matter-lens contribution C_S due to the thermodiffusion of the solutes in the radial temperature field, proportional to Ξ [see Eq. (12)]. In Fig. 3, Ξ is plotted as a function of the mass fraction φ_{KL} of the surfactant (i.e., free KL below the CMC, and free KL plus micellar KL above the CMC), using a linear scale for φ_{KL}. To a good approximation, the $\Xi(\varphi_{KL})$ function can be represented by means of two linear fits,

$$\Xi = (7.82\pm 1.63)\times 10^{-6} - (4.47\pm 0.36)\varphi_{KL}, \tag{15}$$

$$\Xi = -(7.95\pm 1.08)\times 10^{-5} + (4.47\pm 1.93)\times 10^{-4}\varphi_{KL}, \tag{16}$$

below and above the CMC, respectively. Those fits show a discontinuity at the CMC, which will be discussed in Appendix B. The two following sections analyze Ξ before and after the CMC, respectively.

1. KL concentrations below the CMC

The ratio of the numbers of KL and CR molecules is of the order of 2×10^2. Figure 4(a) shows the experimental values of the index of refraction of four solutions as functions of the temperature. These data are used to determine $\partial n/\partial T$, which was found to depend on φ_{KL} [Fig. 4(b)]. It varies from about -1.10×10^{-4} to about -1.25×10^{-4} K^{-1}, and each value was used to calculate the corresponding C_T. The data of Fig. 4(a) were also used to determine $\partial n/\partial\varphi_{KL}$, which was found to be 0.18 ± 0.01. The measured optical absorbance of the aqueous solution of KL and CR at φ_{CR}^* is the same as that of the solution without the KL. The thermal conductivity of the different samples was measured and we found $\kappa\simeq\kappa_w$ for all the samples. With these values we can calculate the nondimensional parameters C_T for all the aqueous solutions of KL and the dye.

In the present section, the solutes are i=CR and KL. The matter-lens signal is given by

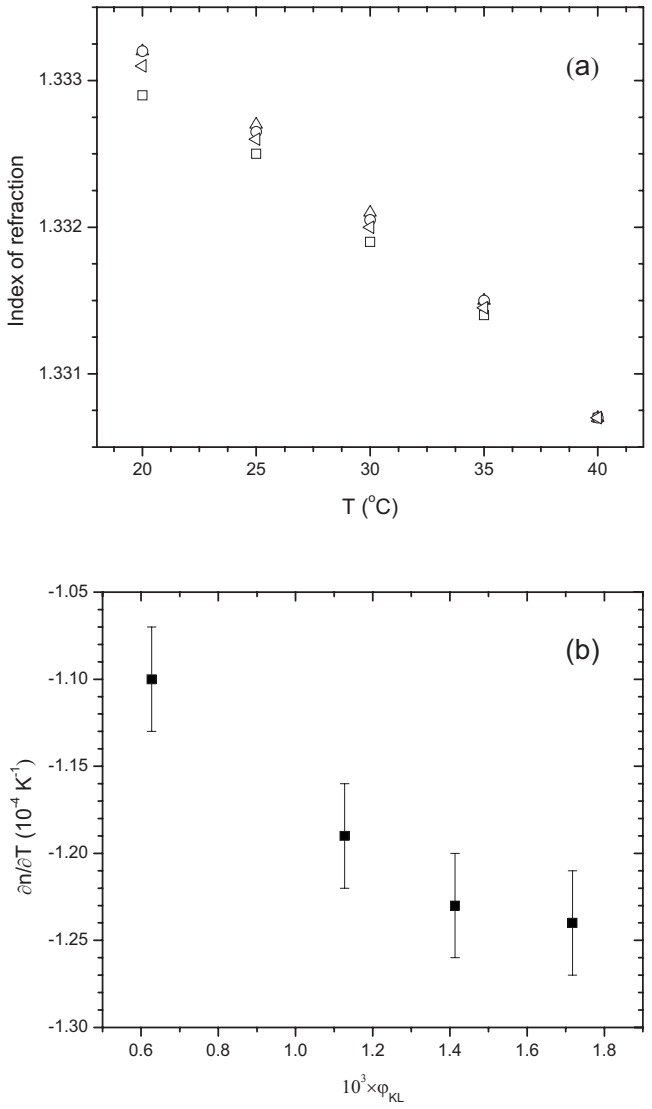

FIG. 4. (a) Index of refraction of aqueous solutions of KL and CR, below the CMC, as a function of the temperature: φ_{KL} = (□) 0.63×10^{-3}; (◁) 1.13×10^{-3}; (○) 1.41×10^{-3}; (△) 1.72×10^{-3}. (b) $\partial n/\partial T$ as a function of φ_{KL}.

$$\Xi = F_{S,CR}\frac{\partial n}{\partial \varphi_{CR}} + F_{S,KL}\frac{\partial n}{\partial \varphi_{KL}}, \tag{17}$$

where $F_{S,CR}$ and $F_{S,KL}$ are the Soret functions of CR and KL. From the phenomenological thermodiffusion equations of Appendix A, those functions can be expressed as

$$F_{S,CR} \approx \frac{D_{T,CR}}{D_{CR}}\varphi^*_{CR} - \frac{D_{CR,KL}}{D_{CR}}\frac{D_{T,KL}}{D_{KL}}\varphi_{KL}, \tag{18}$$

$$F_{S,KL} \approx \frac{D_{T,KL}}{D_{KL}}\varphi_{KL} - \frac{D_{KL,CR}}{D_{KL}}\frac{D_{T,CR}}{D_{CR}}\varphi^*_{CR}, \tag{19}$$

where it is assumed that the nondiagonal diffusivities are weak enough to neglect the product $D_{CR,KL}D_{KL,CR}$ with respect to $D_{CR}D_{KL}$. Each Soret function has a term proportional to the mass fraction of the solute and a correction term due to the diffusion coupling to the other solute. When KL dominates CR, $F_{S,KL}$ is expected to be little affected by the CR fraction. Since the available experimental points are such that $\varphi_{KL} \gg \varphi^*_{CR}$, one can simplify the Soret functions to

$$F_{S,CR} \approx S_{T,CR}\varphi^*_{CR} - \frac{D_{CR,KL}}{D_{CR}}S_{T,KL}\varphi_{KL},$$

$$F_{S,KL} \approx S_{T,KL}\varphi_{KL},$$

letting $S_{T,CR}=D_{T,CR}/D_{CR}$ and $S_{T,KL}=D_{T,KL}/D_{KL}$. A linear relationship $\Xi = a + b\varphi_{KL}$ is obtained where

$$a = S_{T,CR}\varphi^*_{CR}\left(\frac{\partial n}{\partial \varphi_{CR}}\right), \tag{20}$$

$$b = S_{T,KL}\left[\left(\frac{\partial n}{\partial \varphi_{KL}}\right) - \frac{D_{CR,KL}}{D_{CR}}\left(\frac{\partial n}{\partial \varphi_{CR}}\right)\right]. \tag{21}$$

This is consistent with the experimental plot [Eq. (15)]. From a we get the value $S_{T,CR}=0.55\ \mathrm{K}^{-1}$. In the aqueous solution of CR, we found $S_{T,CR}=0.75\ \mathrm{K}^{-1}$. We consider that the agreement is reasonable in view of the approximation of constancy of the diffusivities and the omission of $D_{KL,CR}/D_{KL}$. The slope b yields an equation with two unknowns,

$$-4.47\times10^{-2} = S_{T,KL}\left(0.18 - 0.511\frac{D_{CR,KL}}{D_{CR}}\right). \tag{22}$$

As $S_{T,KL}$ also plays a role above the CMC, we now turn to that concentration range.

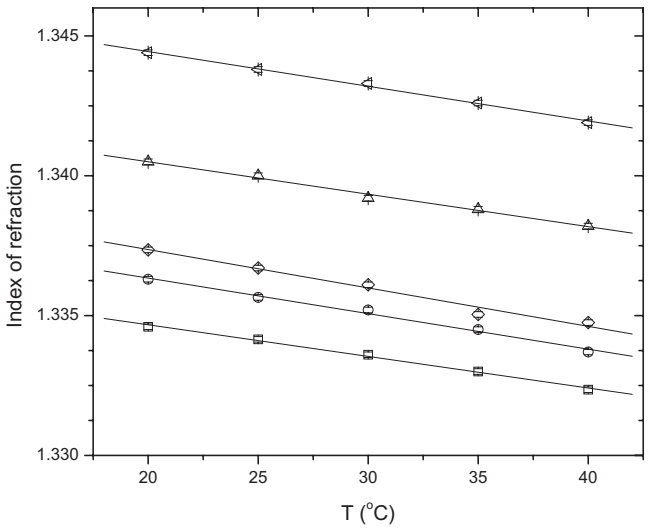

FIG. 5. Index of refraction of aqueous solutions of KL and CR, with φ_{KL} above the CMC, as a function of the temperature: c_{KL} = (□) $0.04M$; (○) $0.08M$; (◇) $0.12M$; (△) $0.20M$; (◁) $0.32M$.

2. KL concentrations above the CMC

Figure 5 shows the index of refraction of aqueous solutions of KL and CR, with φ_{KL} above the CMC, as a function of the temperature. These data were also used to determine $\partial n/\partial c_{KL}$, with c_{KL} denoting the molar concentration of KL.

The measured values of $\partial n/\partial T$ and $\partial n/\partial c_{KL}$ are $-(1.22\pm0.02)\times10^{-4}$ K^{-1} and $(3.49\pm0.05)\times10^{-2}M^{-1}$, respectively. The measured optical absorbance of the aqueous solution of CR and free and micellar KL, at $c_{CR}=40$ μM, is the same as the one measured in the solution without KL. The ratio of the total number of KL molecules (either free or bound in micelles) to the number of CR molecules is of the order of 10^3-10^4. The thermal conductivity of the different samples was measured by using the ZS data and the thermal-lens model, and we found an empirical (fitting) expression $\kappa_{KL}=\kappa_w[0.332\times\exp(-8.2215\times c_{KL})-0.668]$ W m^{-1} K^{-1}. With these values we can calculate the nondimensional parameters C_T for all the aqueous solutions of KL and the dye. The ZS experiment gives access to Ξ through C_S.

Above the CMC, we introduce the approximation of a quasiternary mixture (water, free KL, and micelles), omitting the CR. Then,

$$\Xi = F_{S,KL}\left(\frac{\partial n}{\partial \varphi_{KL}}\right) + F_{S,m}\left(\frac{\partial n}{\partial \varphi_m}\right). \tag{23}$$

We use the same reasoning as previously in order to reduce the number of transport parameters, keeping only the most pertinent ones: KL abounds whereas there are few micelles. Therefore, transport of KL is almost unaffected by the micelles ($D_{KL,m}\approx0$),

$$F_{S,KL} \approx S_{T,KL}\varphi_c, \tag{24}$$

given that the mass fraction of KL stays equal to its value at the CMC. In contrast, the transport of the few micelles can be affected by the presence of abundant KL,

$$F_{S,m} \approx S_{T,m}\varphi_m - \frac{D_{m,KL}}{D_m}S_{T,KL}\varphi_c, \tag{25}$$

where $\varphi_m=\varphi_{KL}-\varphi_c$ and we let $S_{T,m}=D_{T,m}/D_m$. We obtain $\Xi=\alpha+\beta\varphi_{KL}$, where

$$\alpha = \varphi_c\left[S_{T,KL}\left(\frac{\partial n}{\partial \varphi_{KL}}\right) - \left(S_{T,m} + \frac{D_{m,KL}}{D_m}S_{T,KL}\right)\left(\frac{\partial n}{\partial \varphi_m}\right)\right], \tag{26}$$

$$\beta = S_{T,m}\left(\frac{\partial n}{\partial \varphi_m}\right). \tag{27}$$

This is consistent with the experimental plot of $\Xi(\varphi_{KL})$ above the CMC, namely, Eq. (16). From β we get $S_{T,m}=(3.2\pm1.6)\times10^{-3}$ K^{-1}. Expressing $\alpha/\varphi_c+\beta$ yields an equation with two unknowns,

$$-1.28\times10^{-2} = S_{T,KL}\left(0.18 - 0.14\frac{D_{m,KL}}{D_m}\right). \tag{28}$$

Summarizing our findings, we have obtained two equations, (22) and (28), with three unknowns, namely, $S_{T,KL}$, $D_{CR,KL}/D_{CR}$, and $D_{m,KL}/D_m$. We do not have enough information to determine each unknown exactly. Let us pause here before continuing the resolution. In the single-solute case there are two transport parameters, D and D_T, and the ZS method determines $S_T=D_T/D$. So the method determines D_T if D is known independently. In the N-solute case, there are N^2+N transport parameters. If we can vary the mass fraction φ_i of each solute i and measure the ensuing $\partial\Xi/\partial\varphi_i$, then the measurement of Ξ will determine the N thermodiffusion coefficients ($D_{T,i}$) provided that the diffusion matrix ($D_{i,j}$) is known independently. In the present system, this is not the case. Some of the diffusivities (e.g., $D_{KL,CR}$ and $D_{KL,m}$) play a negligible role because the transport of the surfactant is little affected by the few dye molecules or micelles. Yet we still have too many parameters compared to the experimental data. However, it is possible to estimate $S_{T,KL}$. We shall make two hypotheses, and notice that they entail the same sign and order of magnitude for $S_{T,KL}$, together with the same qualitative picture.

As the first hypothesis, consider that KL hardly affects the transport of CR below the CMC, i.e., $D_{CR,KL}\approx0$. Then we get $S_{T,KL}=-2.5\times10^{-1}$ K^{-1} and $D_{m,KL}/D_m=0.92$. As the second hypothesis, consider that KL hardly affects the transport of the micelles above the CMC, i.e., $D_{m,KL}\approx0$. Then we get $S_{T,KL}=-7.1\times10^{-2}$ K^{-1} and $D_{CR,KL}/D_{CR}=0.88$.

In each case, the nondiagonal diffusivity is less than the diagonal one, whereby our neglect of products of nondiagonal diffusivities is justified (remember that $D_{KL,CR}$ and $D_{KL,m}$ were taken to be weak because the CR and micelle concentrations are small compared to that of KL). As for $S_{T,KL}$, the two estimations have the same sign and differ by a factor of 3. In what follows, we shall retain the first estimation, namely, $S_{T,KL}\approx-2.5\times10^{-1}$ K^{-1}. This is because, in the elementary theory of coupled diffusion (see Appendix A), $D_{m,KL}\propto\varphi_m$ and $D_{CR,KL}\propto\varphi_{CR}$, and the lowest $\varphi_m=4\times10^{-3}$ greatly exceeds $\varphi_{CR}^*=2.8\times10^{-5}$. The following section interprets the values found for $S_{T,KL}$ and $S_{T,m}$.

3. Interpretation of $S_{T,KL}$ and $S_{T,m}$

In the previous section we have been able to estimate $S_{T,KL}\approx-2.5\times10^{-1}$ K^{-1} and to determine $S_{T,m}=(3.2\pm1.6)\times10^{-3}$ K^{-1}. The value of $S_{T,m}$ agrees in sign and order of magnitude with that measured in a similar isotropic lyotropic mixture by means of the ZS technique [26], namely, $\approx5.5\times10^{-3}$ K^{-1} in a mixture of water, 1-decanol, and KL. Arnaud and Georges [22] used thermal-lens spectroscopy to investigate the Soret effect of Brij 35 in aqueous solutions. They observed a higher concentration of micelles in the colder region of the sample, consistent with the sign of $S_{T,m}$ found here. Piazza and Guarino [24] reported on experimental results on the Soret effect of micelles in solutions of sodium dodecyl sulfate and NaCl in water. The Soret coefficient was found to be positive and dependent on the amphiphile concentration. All these results indicate that, despite the differences in the micellar systems investigated, the micelles show a thermophobic behavior.

On the other hand, unlike the micelles, the free KL molecules were found to show a thermophilic behavior according to the terminology of the Soret effect. The discrepancy between the responses of the surfactant and the micelles to a temperature gradient is only apparent, as one of us has shown elsewhere [32]. In the single-solute case, the phenomenological equation defining D_T is a biased diffusion equa-

tion (also called a drift-diffusion or migration-diffusion equation), where the drift velocity is

$$\mathbf{v}_d = -\frac{D}{T}\left(TS_T - \frac{d\ln D}{d\ln T}\right)\boldsymbol{\nabla} T, \tag{29}$$

and $d\ln D/d\ln T$ can be estimated from the Stokes-Einstein formula to be about +8.2 in water at 25 °C. At the particle level, we are dealing with a biased random walk whose centroid moves at $\mathbf{v}_d$ and whose variance grows at a rate $2D$ per space dimension [32]. Given that $TS_{T,m}=+(0.95\pm0.47)$, the motion of the micelles (referred to as thermophoresis) occurs *along* $\boldsymbol{\nabla}T$ according to Eq. (29), i.e., toward warmer T. The fact that the micelles accumulate in the region of colder T (reflected in $S_{T,m}>0$) is due to the larger diffusivity in the warmer region, which prevents them from gathering there. Therefore thermodiffusion may be viewed as the superposition of a drift effect and a differential diffusion effect, according to $D_T=-v_d/\nabla T+dD/dT$. In other words, thermodiffusion (transport, embodied in a current density) should not be confused with thermophoresis (motion, embodied in a velocity) [32]. When v_d is weak, the temperature dependence dD/dT of diffusivity prevails in D_T. Thus, if we consider the thermophoretic velocities v_d, the behavior of the micelles is qualitatively similar to that of the surfactant molecules, whatever the estimation of $TS_{T,KL}\approx-21$ to -74. While both the surfactant and the micelles tend to drift toward the warmer region, they differ in the weaker sensitivity of the micelles to ∇T.

So far our analysis has been purely phenomenological, with no appeal to any specific theory or mechanism. We can account for the observed weaker sensitivity of the micelles to ∇T in the frame of a specific theory which correctly described the thermodiffusion of colloidal particles in ionic ferrofluids [33], and was rederived recently [34]. At a low micellar mass fraction φ_m, the theoretical formula is

$$TS_{T,m} = 1 + \left[\frac{\partial U}{\partial(kT)}\right]_{\varphi_m}, \tag{30}$$

where $U(T,\varphi_m)$ is the energy of interaction of a micelle with its surroundings, and k is the Boltzmann constant. Since $[\partial U/\partial(kT)]_{\varphi_m}=-(0.05\pm0.47)$, this suggests that U is low in the case of micelles. In contrast, $TS_{T,KL}\approx-74$ implies $[\partial U/\partial(kT)]_{\varphi_{KL}}\approx-75$. Now KL in a *trans* configuration may be sketched as a cylinder of 1.7 nm length and 0.5 nm diameter, while the micelles have about 100 molecules and may be sketched as spheres of 10 nm diameter. Surfactant molecules and micelles strongly differ with respect to their interaction with water. Surfactant molecules are amphiphiles (with polar and nonpolar groups in the same molecule) and the KL aggregated in direct micelles exposes the polar group to the water molecules, thereby preventing contact of the paraffinic chains with water. One thus understands that the micellization reduces the interaction energy U of the ball of KL molecules with the solvent. This, in turn, reduces the interaction contribution to TS_T in Eq. (30), consistent with the finding $[\partial U/\partial(kT)]_{\varphi_m}=-0.05$ instead of $[\partial U/\partial(kT)]_{\varphi_{KL}}\approx-75$. It is noteworthy that the chemical dissimilarity between the surfactant molecules and the micelles caused by the micellization entails an interaction between them, accounting for a nonvanishing value of $D_{m,KL}$ (see Appendix B), but we do not know of a model predicting that value.

V. CONCLUSIONS

In this paper, we have shown that the Z-scan technique and a generalization of the thermal-lens model described in Ref. [26] can be used to investigate the Soret effect. The technique allows one to isolate a matter-lens contribution Ξ which is a linear combination of the mass gradients. The phenomenology of multicomponent thermodiffusion expresses Ξ as a function of thermodiffusion and diffusion coefficients (both diagonal and nondiagonal). If the latter coefficients are known independently, the former are inferred from $\partial\Xi/\partial\varphi_i$. Otherwise, Soret ratios can be obtained within certain limits. The method, which combines the Z-scan technique and the phenomenology of multicomponent thermodiffusion, is not restricted to the particular system considered in this paper, and it can be applied to study thermodiffusion in any complex fluid. We have found that the response of the mixture of amphiphilic molecules and water is sensitive to the aggregation state of that mixture. The matter-lens signal $\Xi(\varphi_{KL})$ exhibits a sharp variation around the CMC. The jump in Ξ just above the CMC is due to the nondiagonal diffusivity $D_{m,KL}$ expressing the sensitivity of micelle diffusion to the gradient in the mass fraction of free KL. The change in the slope $\partial\Xi/\partial\varphi_{KL}$ is due to the very different Soret ratios of the surfactant and the micelles. Although the Soret ratios have opposite signs, the thermophoreses of both species occur toward warmer temperatures. The sharp difference in the Soret ratios endows $\Xi(\varphi_{KL})$ with the capacity of evidencing the micelle formation in the lyotropic mixture and determining the CMC.

ACKNOWLEDGMENTS

We are indebted to FAPESP (Fundação de Amparo à Pesquisa do Estado de São Paulo), CAPES (Fundação Coordenação Aperfeiçoamento de Pessoal de Nível Superior—MEC), and CNPq (Instituto do Milênio de Fluidos Complexos—IMFCx) for financial support.

APPENDIX A

In an isothermal multicomponent solution, it is known [35–37] that the diffusion of a solute 1 may be affected by that of cosolutes 2,3, … , and conversely. This is manifested in nondiagonal diffusivities D_{ij} in addition to the usual (diagonal) diffusivities D_{ii},

$$\mathbf{j}_1 = -D_{11}\boldsymbol{\nabla}\varphi_1 - D_{12}\boldsymbol{\nabla}\varphi_2 - D_{13}\boldsymbol{\nabla}\varphi_3\ldots, \tag{A1}$$

$$\mathbf{j}_2 = -D_{21}\boldsymbol{\nabla}\varphi_1 - D_{22}\boldsymbol{\nabla}\varphi_2 - D_{23}\boldsymbol{\nabla}\varphi_3\ldots, \tag{A2}$$

etc. The nondiagonal D_{ij} refers to the dependence of current density $\mathbf{j}_i$ of species i on the gradient $\boldsymbol{\nabla}\varphi_j$ of species $j\neq i$. While in most problems D_{ii} may be taken as independent of φ_i to a very good approximation, this is *not* true of D_{ij}. If $\varphi_i\to0$, there can be no current of species i even though $\boldsymbol{\nabla}\varphi_j$

takes important values. Therefore D_{ij} is a function of φ_i that vanishes with φ_i. This can be seen in the elementary theory of nondiagonal diffusivities, where $\mathbf{j}_i$ is proportional to φ_i and to the gradient of the chemical potential of species i. That chemical potential depends on φ_j because the solution is not ideal in the thermodynamical sense [35]: there is an interaction between i and j, in which the solvent also plays a role. This interaction is the reason why a gradient of species j entails a flow of i. In the present paper, we approximate D_{ij} to a constant value as long as φ_i does not take vanishingly low values. Therefore, in Eqs. (A1) and (A2) $\mathbf{j}_i$ is treated as a linear combination of the gradients with *constant* coefficients.

Note that most presentations of multicomponent diffusion are based upon the *mixture* framework, where all the components 0,1,2,3, … are treated on the same footing. Instead, we use the *solution* framework, where the solvent 0 is treated differently, owing to its abundance ($\varphi_0 \approx 1$). Its transport $\mathbf{j}_0$ is not considered. Also, note that expressions (A1) and (A2) of the current densities are not modified by a possible dynamic exchange equilibrium between species 1 and 2. Such an exchange is manifested as a contribution to $\partial\varphi_i/\partial t$ adding up to $-\boldsymbol{\nabla}\cdot\mathbf{j}_i$ in the right-hand side of the continuity equation for species i. The steady state $\partial\varphi_i/\partial t=0$ hardly differs from $\mathbf{j}_i=\mathbf{0}$ if the exchange takes place on a time scale of the order of a millisecond. This comes about because at the particle level diffusion is a random walk whose steps have a typical time scale equal to the momentum-relaxation time. The latter is estimated from the Stokes-Einstein formula to be $M/6\pi\eta R$, with M the mass of the diffusing particle, R its radius, and η the dynamical viscosity of the solvent. Whether we are considering free KL or a micelle, the diffusion time step is always much shorter than a millisecond. As far as thermodiffusion is concerned, it only adds up a bias to the random walk, making it asymmetric without changing its intrinsic time scale $M/6\pi\eta R$.

In Eqs. (A1) and (A2), the lesser importance of nondiagonal diffusivities is expected from the necessary positivity of the diffusion matrix, which requires, for instance, $D_{11}D_{22}-D_{12}D_{21}>0$. This is indeed found in experimental determinations of diffusion matrices [35].

When the multicomponent solution is not isothermal, the structure of the phenomenological current equations is necessarily [35–37] as follows:

$$\mathbf{j}_1 = -D_{11}\boldsymbol{\nabla}\varphi_1 - D_{12}\boldsymbol{\nabla}\varphi_2 - D_{13}\boldsymbol{\nabla}\varphi_3 \cdots - \varphi_1 D_{T,1}\boldsymbol{\nabla}T, \tag{A3}$$

$$\mathbf{j}_2 = -D_{21}\boldsymbol{\nabla}\varphi_1 - D_{22}\boldsymbol{\nabla}\varphi_2 - D_{23}\boldsymbol{\nabla}\varphi_3 \cdots - \varphi_2 D_{T,2}\boldsymbol{\nabla}T, \tag{A4}$$

etc. Each diffusion current is supplemented by a term proportional to $\boldsymbol{\nabla}T$ and to the mass fraction of the solute, involving a thermodiffusion coefficient $D_{T,i}$.

To see the change in the Soret effect of a species induced by the diffusion coupling to other species, we shall solve Eqs. (A3) and (A4) for the case of two solutes. In the steady state, the vanishing of the currents yields a linear system of two equations with the unknowns $\boldsymbol{\nabla}\varphi_1$ and $\boldsymbol{\nabla}\varphi_2$. The solution is

$$\boldsymbol{\nabla}\varphi_1 = -\frac{\varphi_1 D_{T,1}D_{22} - \varphi_2 D_{T,2}D_{12}}{D_{11}D_{22} - D_{12}D_{21}}\boldsymbol{\nabla}T, \tag{A5}$$

and similarly for $\boldsymbol{\nabla}\varphi_2$, owing to the symmetrical roles of 1 and 2. The Soret function $F_{S,1}$ of 1, defined as the steady-state value of $-\boldsymbol{\nabla}\varphi_1/\boldsymbol{\nabla}T$, is

$$F_{S,1}(\varphi_1,\varphi_2) = \frac{\varphi_1 D_{T,1}D_{22} - \varphi_2 D_{T,2}D_{12}}{D_{11}D_{22} - D_{12}D_{21}}. \tag{A6}$$

Expression (A6) shows that, in general, the Soret function of solute 1 will depend on the transport properties and mass fractions of cosolutes 2,3, …. Two limiting cases are worth treating. First, consider that $\varphi_2 \ll \varphi_1$ and $|D_{T,2}| \ll |D_{T,1}|$. Then,

$$F_{S,1} \approx \frac{D_{T,1}}{D_{11}}\varphi_1 \tag{A7}$$

is linear in φ_1, with the usual Soret coefficient $D_{T,1}/D_{11}$. The change due to the cosolute is of relative order $|D_{12}|/D_{11} \lesssim 1$. Second, consider that $\varphi_2|D_{T,2}| \gg \varphi_1|D_{T,1}|$ and $D_{12}\neq 0$. Then,

$$F_{S,1} \approx \frac{D_{T,2}}{D_{22}}\left(-\frac{D_{12}}{D_{11}}\right)\varphi_2. \tag{A8}$$

In this case, $F_{S,1}$ is proportional to φ_2 instead of φ_1, with the following two prefactors: (i) the effective Soret coefficient $D_{T,2}/D_{22}$ of the cosolute, and (ii) a relative strength of diffusion coupling, $-D_{12}/D_{11}$. The Soret effect of 1 is largely governed by the transport properties of 2. Since nondiagonal diffusivities can have both signs, even the sign of $F_{S,1}$ can be changed by the diffusive coupling to the cosolute(s).

From Eq. (A6), the ZS observable $\Xi = F_{S,1}(\partial n/\partial\varphi_1) + F_{S,2}(\partial n/\partial\varphi_2)$ will be, in general, a linear combination of the mass fractions φ_1 and φ_2. Again, we consider the limiting cases of weak and strong diffusion coupling. If the transports of 1 and 2 are weakly coupled, (i.e., D_{12} and $D_{21} \approx 0$), the combination simplifies to

$$\Xi = \left(\frac{\partial n}{\partial\varphi_1}\right)\left(\frac{D_{T,1}}{D_{11}}\right)\varphi_1 + \left(\frac{\partial n}{\partial\varphi_2}\right)\left(\frac{D_{T,2}}{D_{22}}\right)\varphi_2. \tag{A9}$$

If the transport of 1 is controlled by 2, we expect, from Eq. (A8),

$$\Xi = \left[\left(\frac{\partial n}{\partial\varphi_1}\right)\left(-\frac{D_{12}}{D_{11}}\right) + \left(\frac{\partial n}{\partial\varphi_2}\right)\right]\left(\frac{D_{T,2}}{D_{22}}\right)\varphi_2, \tag{A10}$$

i.e., $\Xi \propto \varphi_2$, and vice versa if $1 \leftrightarrow 2$. Consequently, the plot of Ξ versus φ_2 allows us to detect whether the transports are coupled or not.

APPENDIX B

The aim of this appendix is to establish the phenomenological formula for the variation in Ξ as the CMC is crossed. It is based on the approximate expressions of Ξ used in Sec. IV B 2. Below the CMC, Ξ is

$$\Xi_- = \left(S_{T,CR}\varphi_{CR}^* - \frac{D_{CR,KL}}{D_{CR}} S_{T,KL}\varphi_{KL} \right) \left(\frac{\partial n}{\partial \varphi_{CR}} \right) + S_{T,KL}\varphi_{KL} \left(\frac{\partial n}{\partial \varphi_{KL}} \right), \tag{B1}$$

where $\varphi_{KL}=\varphi_c$. The contribution in φ_{CR}^* is then expected to be negligible, whence

$$\Xi_- \approx \left[-\frac{D_{CR,KL}}{D_{CR}} \left(\frac{\partial n}{\partial \varphi_{CR}} \right) + \left(\frac{\partial n}{\partial \varphi_{KL}} \right) \right] S_{T,KL}\varphi_c. \tag{B2}$$

Above the CMC, Ξ is

$$\Xi_+ = S_{T,KL}\varphi_c \left(\frac{\partial n}{\partial \varphi_{KL}} \right) + \left(S_{T,m}\varphi_m - \frac{D_{m,KL}}{D_m} S_{T,KL}\varphi_c \right) \left(\frac{\partial n}{\partial \varphi_m} \right). \tag{B3}$$

Clearly the free surfactant contribution is the same in Ξ_- and Ξ_+: it does not cause a discontinuity in Ξ. The variation in Ξ around the CMC is due to (i) the presence of CR below the CMC, as CR transport is controlled by the abundant KL instead of the concentration of CR itself; and (ii) the presence of micelles above the CMC, as their transport is essentially determined by abundant KL in the limit $\varphi_m \to 0$. As a result of Eqs. (B2) and (B3),

$$\Xi_+ - \Xi_- = \left[-\frac{D_{m,KL}}{D_m} \left(\frac{\partial n}{\partial \varphi_m} \right) + \frac{D_{CR,KL}}{D_{CR}} \left(\frac{\partial n}{\partial \varphi_{CR}} \right) \right] S_{T,KL}\varphi_c. \tag{B4}$$

The CR term in $\Xi_+ - \Xi_-$ is due to the fact that CR is taken into account below the CMC while CR is disregarded beyond the CMC in the quasiternary approximation. For consistency, we can write

$$\Xi_+ - \Xi_- \approx -\frac{D_{m,KL}}{D_m} \left(\frac{\partial n}{\partial \varphi_m} \right) S_{T,KL}\varphi_c, \tag{B5}$$

and this is the expression of $\Xi_+ - \Xi_-$ that we shall henceforth discuss.

As noticed in Appendix A, in the limit $\varphi_m \to 0$ the nondiagonal diffusivity $D_{m,KL}$ should vanish. The reason is that isothermal transport of micelles is described by a current density

$$\mathbf{j}_m = -D_m \nabla \varphi_m - D_{m,KL} \nabla \varphi_{KL}. \tag{B6}$$

Now, if $\varphi_m=0$, there are no micelles to be transported, whatever the concentration of KL. To ensure $\mathbf{j}_m=\mathbf{0}$ as $\varphi_m=0$, we should have $D_{m,KL} \to 0$ as $\varphi_m \to 0$. As a result, we expect the discontinuity $\Xi_+ - \Xi_-$ to vanish at the CMC: Ξ should be a continuous function of φ_{KL}. Why is it, then, that the experimental plot of $\Xi(\varphi_{KL})$ suggests otherwise? In our experiment, we do not have enough experimental points to actually check the limit $\varphi_m \to 0$. The lowest value of φ_m is 4×10^{-3}, which is almost twice $\varphi_c=6\times10^{-3}$, so that the actual value of $D_{m,KL}$ is not zero. So $\Xi(\varphi_{KL})$ can be portrayed as a mathematically continuous function exhibiting a sharp variation around the CMC because of the profound change occurring in the system. The observed discontinuity in Ξ refers in fact to the difference in the linear fits before and after the CMC. According to Appendix A, the validity of linear fits excludes the range $\varphi_m \to 0$ where $D_{m,KL}$ significantly varies and drops to zero. Linear fits can be performed because the function $\Xi(\varphi_{KL})$ in the close neighborhood of the CMC is not accessed experimentally.

Finally, the reader can check that, whatever the hypothesis used to calculate $S_{T,KL}$ in Sec. IV B 2, $\Xi_+ - \Xi_-$ keeps the same value according to Eq. (B4). Depending on the hypothesis, the relative strength of diffusion coupling $D_{m,KL}/D_m$ ranges between 0 (KL has no effect on the diffusion of micelles) and 0.92 (the effect of the KL gradient is comparable to that of the micelle gradient). In Sec. IV B 2 we argued that the latter value is more likely.

[1] J. Israelachvili, *Intermolecular and Surface Forces* (Academic Press, San Diego, 1992).

[2] A. M. Figueiredo Neto and S. R. A. Salinas, *The Physics of Lyotropic Liquid Crystals: Phase Transitions and Structural Properties* (Oxford University Press, Oxford, 2005).

[3] C. Tanford, *The Hydrophobic Effect: Formation of Micelles and Biological Membranes* (Wiley, New York, 1980).

[4] L. Leibler, H. Orland, and J. C. Wheeler, J. Chem. Phys. **79**, 3550 (1983).

[5] W. E. McMullen, W. M. Gelbart, and A. Ben-Shaul, J. Phys. Chem. **88**, 6649 (1984).

[6] R. G. Larson *et al.*, J. Chem. Phys. **83**, 2411 (1985).

[7] W. C. Presto, J. Phys. Colloid Chem. **52**, 84 (1948).

[8] F. L. S. Cuppo and A. M. Figueiredo Neto, Langmuir **18**, 9647 (2002). Note: the correct value of the potassium laurate–water CMC is 0.0255*M*.

[9] S. R. de Groot, *L' Effet Soret. Diffusion Thermique dans les Phases Condensées* (Noord-Hollandsche Uitgevers Maatschappij, Amsterdam, 1945).

[10] L. Landau and E. Lifshitz, *Fluid Mechanics* (Pergamon, London, 1959).

[11] P. Costesèque, D. Fargue, and P. Jamet, in *Thermal Nonequilibrium Phenomena in Fluid Mixtures*, edited by W. Köhler and S. Wiegand (Springer, Berlin, 2002).

[12] M. Schimpf, in *Thermal Nonequilibrium Phenomena in Fluid Mixtures*, edited by W. Köhler and S. Wiegand (Springer, Berlin, 2002).

[13] C. Vidal, G. Dewel, and P. Borckmans, *Au-delà de l'Équilibre* (Hermann, Paris, 1994).

[14] E. Blums, G. Kronkalns, and R. Ozols, J. Magn. Magn. Mater. **39**, 142 (1983).

[15] W. Köhler, J. Chem. Phys. **98**, 660 (1993).

[16] J. Lenglet, A. Bourdon, J. C. Bacri, and G. Demouchy, Phys. Rev. E **65**, 031408 (2002).

[17] M. Sheik-Bahae, A. A. Said, and E. W. Van Stryland, Opt. Lett. **14**, 955 (1989).

[18] S. Alves, A. Bourdon, and A. M. Figueiredo Neto, J. Opt. Soc. Am. B **20**, 713 (2003).
[19] R. Rusconi, L. Isa, and R. Piazza, J. Opt. Soc. Am. B **21**, 605 (2004).
[20] S. Duhr and D. Braun, Proc. Natl. Acad. Sci. U.S.A. **103**, 19678 (2006).
[21] J. Georges and T. Paris, Anal. Chim. Acta **386**, 287 (1999).
[22] N. Arnaud and J. Georges, Spectrochim. Acta, Part A **57**, 1085 (2001).
[23] M. Giglio and A. Vendramini, Phys. Rev. Lett. **38**, 26 (1977).
[24] R. Piazza and A. Guarino, Phys. Rev. Lett. **88**, 208302 (2002).
[25] S. Wiegand, J. Phys.: Condens. Matter **16**, R357 (2004).
[26] S. Alves, F. L. S. Cuppo, A. Bourdon, and A. M. Figueiredo Neto, J. Opt. Soc. Am. B **23**, 2328 (2006).
[27] M. Marcoux and M. C. Charrier-Mojtabi, Entropie, No. **218**, 13 (1999).
[28] K. B. Haugen and A. Firoozabadi, J. Chem. Phys. **122**, 014516 (2005).
[29] A. Leahy-Dios, M. M. Bou-Ali, J. K. Platten, and A. Firoozabadi, J. Chem. Phys. **122**, 234502 (2005).
[30] S. I. Alves, A. Bourdon, and A. M. Figueiredo Neto, J. Magn. Magn. Mater. **289**, 285 (2005).
[31] W. U. Malik and A. K. Jain, J. Inorg. Nucl. Chem. **29**, 2825 (1967).
[32] E. Bringuier, Philos. Mag. **87**, 873 (2007).
[33] E. Bringuier and A. Bourdon, Phys. Rev. E **67**, 011404 (2003).
[34] J. K. G. Dhont, S. Wiegand, S. Duhr, and D. Braun, Langmuir **23**, 1674 (2007).
[35] E. L. Cussler, *Diffusion: Mass Transfer in Fluid Systems*, 2nd ed. (Cambridge University Press, Cambridge, U.K., 1997).
[36] J. H. Ferziger and H. G. Kaper, *Mathematical Theory of Transport Processes in Gases* (North-Holland, Amsterdam, 1972).
[37] R. B. Bird, W. E. Stewart, and E. N. Lightfoot, *Transport Phenomena*, 2nd ed. (Wiley, New York, 2002).